Structure of human endo-α-1,2-mannosidase (MANEA), an antiviral host-glycosylation target

Łukasz F. Sobala[a,1], Pearl Z. Fernandes[b,c], Zalihe Hakki[b,c], Andrew J. Thompson[a], Jonathon D. Howe[d], Michelle Hill[d], Nicole Zitzmann[d], Scott Davies[e], Zania Stamataki[e], Terry D. Butters[d], Dominic S. Alonzi[d], Spencer J. Williams[b,c,2], and Gideon J. Davies[a,2]

[a]Department of Chemistry, University of York, York YO10 5DD, United Kingdom; [b]School of Chemistry, University of Melbourne, Parkville, VIC 3010, Australia; [c]Bio21 Molecular Science and Biotechnology Institute, University of Melbourne, Parkville, VIC 3010, Australia; [d]Oxford Glycobiology Institute, Department of Biochemistry, University of Oxford, Oxford OX1 3QU, United Kingdom; and [e]Institute for Immunology and Immunotherapy, University of Birmingham, Birmingham B15 2TT, United Kingdom

Edited by Gerald W. Hart, University of Georgia, Athens, GA, and accepted by Editorial Board Member Brenda A. Schulman September 28, 2020 (received for review July 1, 2020)

Mammalian protein N-linked glycosylation is critical for glycoprotein folding, quality control, trafficking, recognition, and function. N-linked glycans are synthesized from $Glc_3Man_9GlcNAc_2$ precursors that are trimmed and modified in the endoplasmic reticulum (ER) and Golgi apparatus by glycoside hydrolases and glycosyltransferases. Endo-α-1,2-mannosidase (MANEA) is the sole *endo*-acting glycoside hydrolase involved in N-glycan trimming and is located within the Golgi, where it allows ER-escaped glycoproteins to bypass the classical N-glycosylation trimming pathway involving ER glucosidases I and II. There is considerable interest in the use of small molecules that disrupt N-linked glycosylation as therapeutic agents for diseases such as cancer and viral infection. Here we report the structure of the catalytic domain of human MANEA and complexes with substrate-derived inhibitors, which provide insight into dynamic loop movements that occur on substrate binding. We reveal structural features of the human enzyme that explain its substrate preference and the mechanistic basis for catalysis. These structures have inspired the development of new inhibitors that disrupt host protein N-glycan processing of viral glycans and reduce the infectivity of bovine viral diarrhea and dengue viruses in cellular models. These results may contribute to efforts aimed at developing broad-spectrum antiviral agents and help provide a more in-depth understanding of the biology of mammalian glycosylation.

glycosylation | structural biology | secretory pathway | enzyme | antiviral

Asparagine (N)-linked glycosylation is a protein modification that is widespread in eukaryotes and is essential for protein quality control and trafficking (1). N-linked glycans contribute to protein structure and stability, receptor targeting, development, and immune responses (2). N-linked glycosylation occurs in the secretory pathway and is initiated in the lumen of the endoplasmic reticulum (ER) through cotranslational transfer of the triantennary $Glc_3Man_9GlcNAc_2$ glycan from a lipid linked precursor (2–5) (Fig. 1). The formation of mature glycoproteins requires the removal of the glucose residues, typically through the action of α-glucosidases I and II, which are localized within the rough ER. However, in most cell lines and in human patients, genetic disruption of α-glucosidase I or II or inhibition of their activities does not prevent the formation of mature glycoproteins because of the action of Golgi endo-α-1,2-mannosidase (MANEA; mannosidase, endo-alpha) (6), which provides a glucosidase-independent pathway for glycoprotein maturation termed the endomannosidase pathway (7).

MANEA is present chiefly in *cis*/*medial* Golgi (84%) and the ER-Golgi intermediate compartment (15%) (8) and allows trimming of glucosylated mannose residues from $Glc_{1-3}Man_9GlcNAc_2$ structures and B and C branch mannose-trimmed variants (see Fig. 1 for a definition of N-glycan branches). The action of MANEA on $Glc_{1-3}Man_9GlcNAc_2$ results in cleavage of the glucosylated mannose in the A branch, releasing $Glc_{1-3}Man$ and $Man_8GlcNAc_2$; human MANEA acts faster on Glc_1Man than on $Glc_{2,3}Man$ glycans (9). The endomannosidase pathway allows processing of ER-escaped, glucosylated high-mannose glycans on glycoproteins that fold independently of the calnexin/calreticulin folding cycle, allowing them to rejoin the downstream N-glycan maturation pathway. In murine BW6147 cells under normal conditions, flux through the endomannosidase pathway accounts for approximately 15% of total flux through the secretory pathway (10); under conditions of glucosidase blockade through knockout or inhibition, MANEA can support as much as 50% of the normal glycoprotein flux, depending on cellular expression levels (10). MANEA activity accounts for the accumulation of Glc_3Man tetrasaccharide in the urine of a neonate suffering from CDG-IIb, a rare genetic disease caused by a deficiency of ER glucosidase I (11).

Most enveloped viruses (e.g., coronaviruses, retroviruses, ebolaviruses, hepatitis B virus [HBV], influenza viruses) contain

Significance

The glycosylation of proteins is a major protein modification that occurs extensively in eukaryotes. Glycosidases in the secretory pathway that trim N-linked glycans play key roles in protein quality control and in the specific modifications leading to mature glycoproteins. Inhibition of glucosidases in the secretory pathway is a proven therapeutic strategy, that holds great promise in the treatment of viral disease. The enzyme endo-α-1,2-mannosidase (MANEA) provides an alternative processing pathway to evade glucosidase inhibitors. We report the three-dimensional structure of human MANEA and complexes with enzyme inhibitors that we show act as antivirals for bovine viral diarrhea and human dengue viruses. The structure of MANEA will support inhibitor optimization and the development of more potent antivirals.

Author contributions: D.S.A., S.J.W., and G.J.D. designed research; Ł.F.S., P.Z.F., Z.H., A.J.T., J.D.H., M.H., S.D., Z.S., D.S.A., and G.J.D. performed research; P.Z.F., Z.H., T.D.B., and S.J.W. contributed new reagents/analytic tools; Ł.F.S., Z.H., N.Z., D.S.A., S.J.W., and G.J.D. analyzed data; and Ł.F.S., D.S.A., S.J.W., and G.J.D. wrote the paper.

The authors declare no competing interest.

This article is a PNAS Direct Submission. G.W.H. is a guest editor invited by the Editorial Board.

This open access article is distributed under Creative Commons Attribution-NonCommercial-NoDerivatives License 4.0 (CC BY-NC-ND).

[1]Present address: Department of Immunochemistry, Laboratory of Glycobiology, Hirszfeld Institute of Immunology and Experimental Therapy, Polish Academy of Sciences, 53-114 Wrocław, Poland.

[2]To whom correspondence may be addressed. Email: sjwill@unimelb.edu.au or gideon.davies@york.ac.uk.

This article contains supporting information online at https://www.pnas.org/lookup/suppl/doi:10.1073/pnas.2013620117/-/DCSupplemental.

First published November 5, 2020.

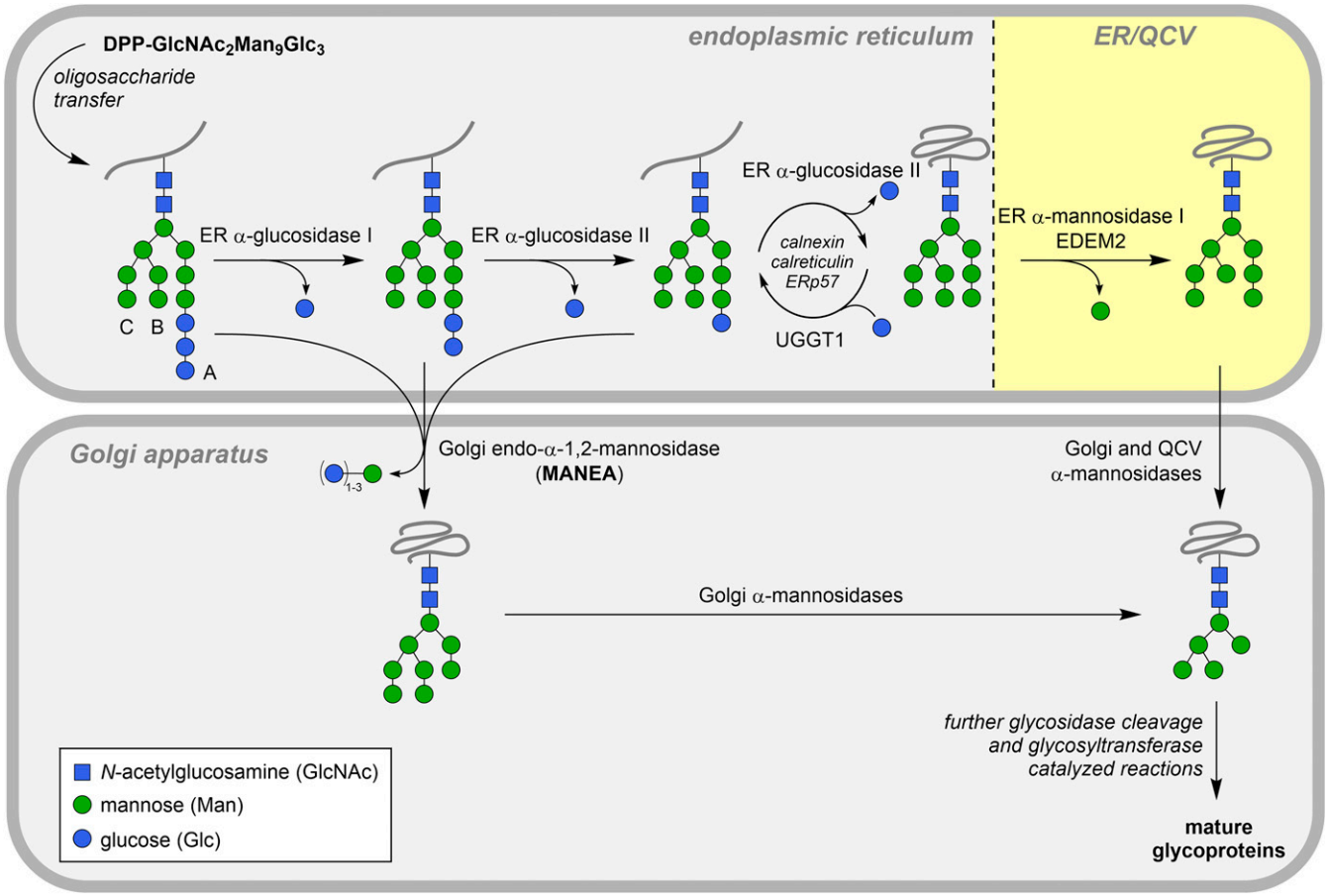

Fig. 1. Simplified pathway for biosynthesis of N-linked glycans through the classical and endomannosidase pathways. En bloc transfer of the preformed $Glc_3Man_9GlcNAc_2$ tetradecasaccharide (branches labeled A/B/C) from the dolichol precursor occurs cotranslationally to Asn residues within the consensus sequence Asn-Xxx-Ser/Thr. Trimming of glucose residues can be achieved through the classical pathway involving sequential action of α-glucosidases I and II. Alternatively, MANEA provides a glucosidase-independent pathway for glycoprotein maturation, through cleaving the glucose-substituted mannose residues. ER mannosidase I resides in quality control vesicles (QCV) (43). ER-associated degradation of terminally misfolded glycoproteins is omitted.

glycoproteins within their envelope (12). Glycosylation is achieved by coopting host cell glycosylation machinery during replication. Substantial efforts have been deployed in the use of inhibitors of α-glucosidases I and II as antivirals (e.g., *N*-butyldeoxynojirimycin, 6-*O*-butanoylcastanospermine) for the treatment of HIV/AIDS (13), dengue (14, 15), and HBV (16, 17) (reviewed in refs. 18–20). Inhibition of host glycosylation pathways, in particular ER glucosidases I and II and Golgi mannosidase I, interferes with the viral lifecycle by impairing protein folding and quality control, inducing the unfolded protein response or mistrafficking of viral glycoproteins. These changes can lead to impairment of secretion (17, 21–23) or fusion (24–26) or evasion of host immunity (27). In the case of HBV, when glucosidases are inhibited, mature HBV viral glycoproteins are still produced through the alternative processing provided by the endomannosidase pathway (23). However, the contribution of the endomannosidase pathway to viral protein assembly under normal conditions remains poorly studied, and the antiviral activity of inhibitors targeting MANEA has not yet been evaluated.

The *Homo sapiens* endo-α-1,2-mannosidase gene, *MANEA*, is located on chromosome 6. The *MANEA* gene gives rise to three transcripts, only one of which encodes the complete protein product, MANEA. MANEA is categorized as a member of the glycoside hydrolase (GH) family 99 in the Carbohydrate-Active enZyme (CAZy) database (28), which also contains bacterial endo-α-1,2-mannanases from *Bacteroides xylanisolvens* (*Bx*GH99) and *Bacteroides thetaiotaomicron* (*Bt*GH99) that act on related structures within yeast mannans and that share ∼40% identity with MANEA (29–31). *MANEA* encodes a 462-aa protein that consists of a single-pass type II membrane protein with a transmembrane helix followed by a stem region, followed by the catalytic domain (32). Here we reveal the structure of the catalytic domain of human MANEA. Through complexes with substrate, we show the architecture of the binding groove and identify key catalytic residues. We report structures with MANEA inhibitors that were designed based on the structure of the glucosylated high-mannose N-glycan. Finally, we show that inhibitors of MANEA act as antiviral agents against bovine viral diarrheal virus (BVDV) and dengue virus (DENV), confirming that MANEA is an antiviral target.

Results

Expression and Activity of Human MANEA GH99. To obtain soluble MANEA protein for structure and function studies to inform inhibitor design, attempts were made to express the gene. A truncated gene for MANEA, consisting of the catalytic domain beyond the stem domain (i.e., residues 98 to 462, hereinafter MANEA-Δ97), was synthesized in codon-optimized form. Expression trials in *Escherichia coli* BL21(DE3) cells yielded only insoluble protein, but we were inspired by a report of soluble expression using cold-shock promotors (pCold-I vector) and coexpression of GroEL chaperones (33). Optimal yields of

soluble MANEA-Δ97 were obtained using Terrific Broth supplemented with glycerol and 20 mM $MgCl_2$, affording ∼2 to 3 mg L^{-1} (*SI Appendix*, Fig. S1*A* and *Experimental Procedures*). The recombinant protein was purified using the encoded N-terminal His_6-tag and was stable, with a T_m of 50 °C (*SI Appendix*, Fig. S1*B*).

Treatment of $Glc Man_9 GlcNAc_2$ with recombinant MANEA-Δ97 released α-Glc-1,3-Man and $Man_8GlcNAc_2$ (*SI Appendix*, Fig. S1*C*). Enzyme kinetics were measured using α-Glc-1,3-α-Man-1,2-α-Man-1,2-α-Man-OMe ($GlcMan_3OMe$) as substrate with a coupled assay in which the product α-1,2-Man-ManOMe is hydrolyzed by α-mannosidase and the resultant mannose quantified using a D-mannose/D-fructose/D-glucose detection kit (Megazyme) (30). MANEA-Δ97 hydrolyzed $GlcMan_3OMe$ with a k_{cat} of 27.7 ± 1.0 min^{-1} and a K_M of 426 ± 33 μm (k_{cat}/K_M of 65 mM^{-1} min^{-1}) (*SI Appendix*, Fig. S1*D*). The catalytic efficiency is similar to that displayed by *Bt*GH99 on the epimeric Man_4OMe substrate (K_M = 2.6 mM; k_{cat} = 180 min^{-1}; k_{cat}/K_M = 69 mM^{-1} min^{-1}) (30). The E404Q variant of MANEA-Δ97 was inactive on this substrate, consistent with the proposed mechanism (34).

Development of MANEA Inhibitors. GlcDMJ, a cell-permeable inhibitor of MANEA (35, 36), is composed of the well-known mannosidase iminosugar inhibitor deoxymannojirimycin (DMJ) modified with a glucosyl residue at the 3-position to enhance specificity and binding to MANEA by mimicking the substrate and benefitting from substrate-enzyme contacts in the −2 subsite (Fig. 2). The related compound GlcIFG (31), which is also cell-permeable (37), was developed through a similar approach applied to the azasugar isofagomine (IFG). Similarly, ManIFG was synthesized to match the substrate stereochemistry of yeast mannan and is a superior inhibitor of bacterial endo-α-1,2-mannanases (30). Because glucosylated mannans are substrates for α-glucosidase II, GlcDMJ and GlcIFG may potentially be degraded in cell-based systems (38), leading to loss of inhibition. Examination of the three-dimensional (3D) X-ray structure of α-glucosidase II in complex with *N*-butyldeoxynojirimycin reveals that binding of the sugar-shaped heterocycle involves a pocket-like active site that will not readily accommodate additional substituents (39). Conversely, it is known that MANEA can cleave $Glc_{1-3}Man$ substrates in which a substituent is tolerated at the 3-position of the glucosylated mannose. Therefore, we synthesized CyMe-GlcIFG, which bears a bulky cyclohexylmethyl substituent at the same position, in the expectation that it should be impervious to α-glucosidase II activity yet still bind to MANEA.

Isothermal titration calorimetry revealed that GlcIFG binds to MANEA-Δ97 with a K_d of 19.6 ± 5.6 nM and to ManIFG with a K_d of 170 ± 32 nM. While we were encouraged by preliminary studies on a bacterial MANEA homolog showing that CyMeGlc-IFG bound better than GlcIFG alone (K_d, 284 nM vs. 625 nM), on the human enzyme, CyMe-GlcIFG bound less tightly than GlcIFG, with a K_d of 929 ± 52 nM (*SI Appendix*, Fig. S1*E*), consistent with structural features observed subsequently (see below). GlcDMJ, previously reported to have IC_{50} values of 1.7 to 5 μM (35, 38), was the weakest binding of the four compounds, with a K_d value of 1,020 ± 36 nM. Thus, MANEA exhibits a preference for inhibitors that match the stereochemistry of the substrate −2/−1 residues (GlcIFG vs. ManIFG), which is the reverse of the preference of bacterial endo-α-1,2-mannanases for the same inhibitors (i.e., for *Bt*GH99: GlcIFG K_d = 625 nM; ManIFG K_d = 140 nM) (30). Consistent with previous findings in bacterial GH99 enzymes, IFG is preferred to DMJ in the −1 subsite.

The 3D Structure of Human MANEA Sheds Light on Eukaryotic Enzyme Specificity. Crystals of human MANEA-Δ97 (Fig. 3*A*) were obtained in several crystal forms (*SI Appendix*, *Experimental Procedures*). The initial crystal form, in space group $P2_12_12$, diffracted to ∼2.25 Å resolution, and structure solution by molecular replacement (using *Bx*GH99 as a search model) was successful, leading to structures with R/R_{free} 18%/22% (*SI Appendix*, Table S1). Unfortunately, this crystal form suffered from occlusion of the active center by the His_6-tag and a metal ion assumed to be Ni^{2+}. A second crystal form, $P4_32_12$, provided data of lower resolution (3 Å), but in this case we could build a loop (131 to 141) absent in the first crystal form; however, this crystal form could not be reliably reproduced. A third crystal form in space group $P6_2$ was obtained with Anderson–Evans polyoxotungstate $[TeW_6O_{24}]^{6-}$ (TEW), which has been used on

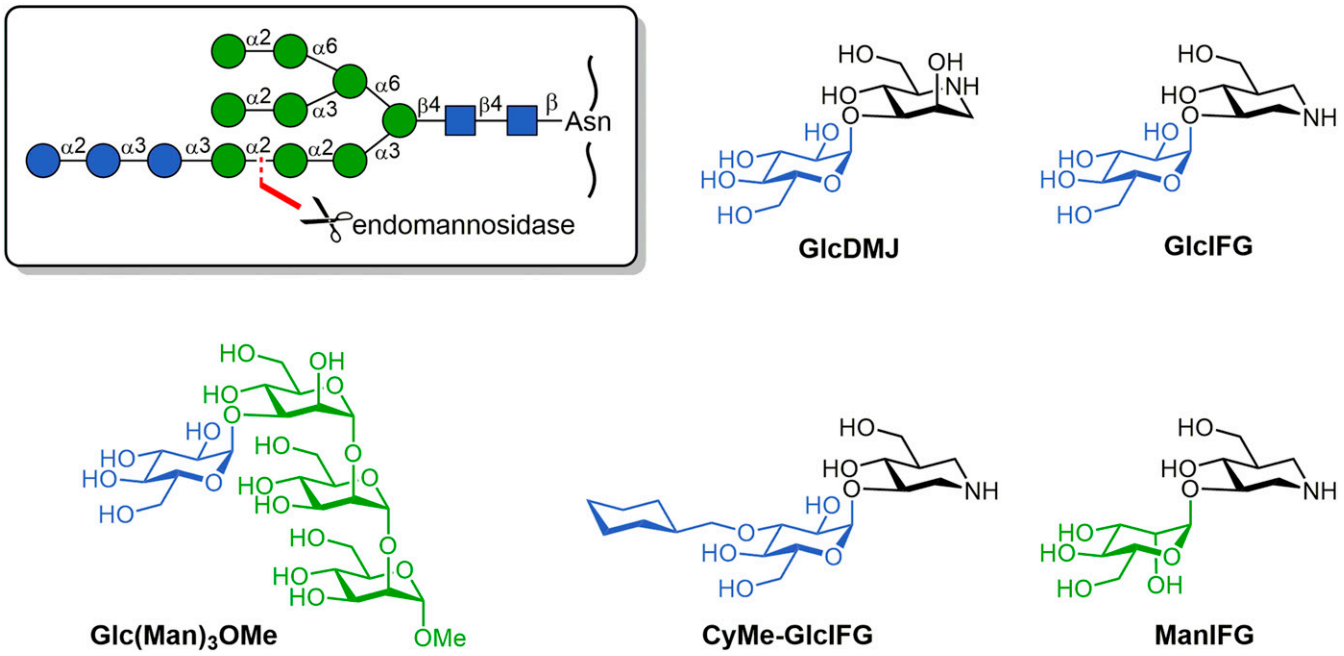

Fig. 2. Substrates and inhibitors for MANEA inspired from the structure of the glucosylated N-glycan substrate. (*Inset*) Structure of $Glc_3Man_9GlcNAc_2$ showing the cleavage site of MANEA.

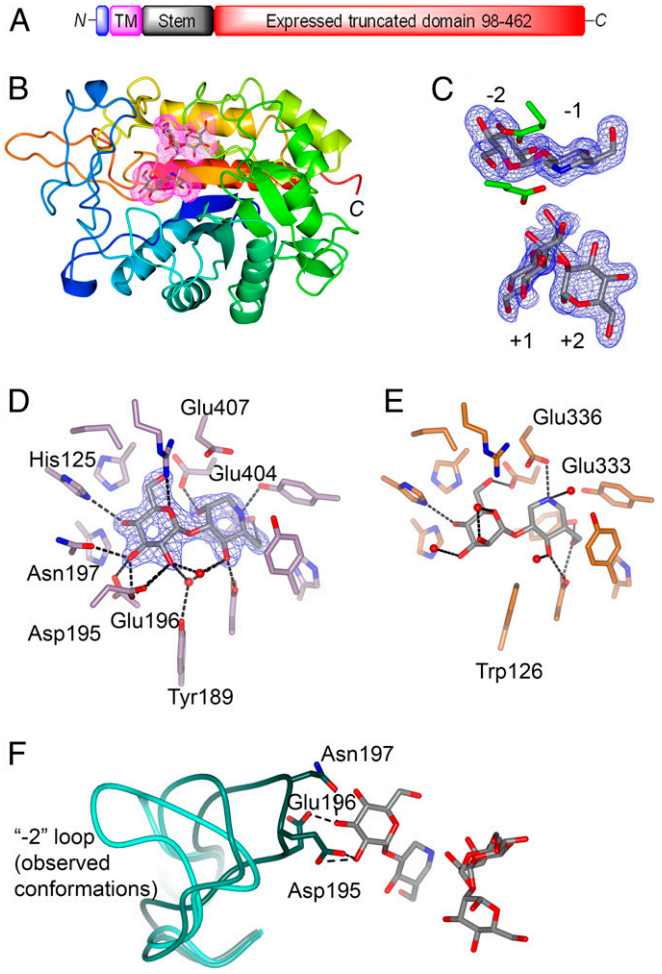

Fig. 3. 3D X-ray structure of *H. sapiens* MANEA endomannosidase and its complexes. (*A*) Domain structure of MANEA indicating the 98 to 462 domain that was expressed. (*B*) 3D structure of MANEA, color-ramped from N (blue) to C (red) terminus and with GlcIFG and α-1,2-mannobiose ligands shaded. (*C*) Electron density for the ternary complex of MANEA with GlcIFG and α-1,2-mannobiose. 2m*Fo*-D*Fc* synthesis contoured at 0.4 $e^{-}/Å^3$. (*D*) The –2 and –1 subsites of MANEA in complex with GlcDMJ, showing the interactions and with key residues labeled. 2m*Fo*-D*Fc* synthesis contoured at 0.6 $e^{-}/Å^3$. (*E*) The comparable –2 and –1 subsites of the bacterial endomannanase *Bx*GH99 involved in yeast mannan degradation, in complex with ManIFG (Protein Data Bank ID code 4V27). (*F*) Residues 189 to 203 containing the flexible loop as observed in the MANEA-E404Q structure (cyan), MANEA+Ni^{2+} structure (darker cyan), and MANEA with GlcIFG and α-1,2 mannobiose structure (darkest cyan; ligand: gray). Hydrogen bonds with the –2 sugar are shown as dashed lines.

occasion in protein crystallography to act as a linking agent between molecules in the crystal lattice; examples include Protein Data Bank ID codes 4OUA, 4PHI, 4Z13, 6G3S, 6QSE, and 6N90 (reviewed in ref. 40). The new crystal form diffracted up to 1.8 Å resolution, generating largely anisotropic datasets. The ligand-binding site was occupied by HEPES, with residues 191 to 201 poised to accept –2/–1 subsite ligands and +1/+2 subsites open. The HEPES molecule was readily replaced by ligand soaking (the IC_{50} for HEPES shows weak binding; *SI Appendix*, Fig. S2), and we obtained a series of complexes including a binary complex of MANEA-Δ97 with GlcIFG, a ternary complex with GlcIFG and α-1,2-mannobiose (structure and refinement statistics in *SI Appendix*, Table S1) and a complex of an inactive E404Q variant with a tetrasaccharide substrate.

The overall 3D structure of human MANEA is a single domain $(\beta/\alpha)_8$ barrel with a (partially; see below) open active center in which Glu404 and Glu407 (human numbering, as part of a conserved **E**W**H**E motif) are the catalytic residues in a neighboring group participation mechanism that proceeds through an epoxide intermediate (34) (Fig. 3 *B* and *C*). The structure is similar (Cα rmsd >0.9 Å over 333 matched residues) to structures reported for *Bt*GH99 and *Bx*GH99 (31), with which MANEA shares 40% sequence identity. The positions of the –2 to +2 ligands in the bacterial and human GH99 proteins are equivalent and the sugar interactions in the –2 to +2 subsites, all of which bind mannosides with identical linkages in both high-mannose N-glycans (MANEA) and yeast mannan (bacterial *endo*-α-1,2-mannanases) (29) are invariant.

A key difference between the substrates for the human and bacterial GH99 enzymes are the –2 sugar residues, which is glucose in high-mannose N-glycans, and mannose in yeast mannan. These differences are achieved by differences in recognition between the human and bacterial GH99 enzymes in the –2 subsite and its environs. In bacterial endo-α-1,2-mannanases, Trp126 (numbering for *Bx*GH99) (31) forms a hydrophobic interaction with the C2 that was believed to be responsible for the selectivity of bacterial enzymes for ManMan vs. GlcMan substrates. In MANEA, the equivalent residue is Tyr189, which makes a water-mediated interaction with O2 of Glc in the –2 subsite (Fig. 3 *D* and *E*). Notably, we observed a loop (residues 191 to 201, hereinafter the "–2 loop"), absent in the bacterial structures, that was flexible and observed in different positions in the different MANEA crystal forms (Fig. 3*F*).

Two residues within the –2 loop are invariant across animal MANEAs: Asp195 and Gly198. Our structures reveal that Asp195 forms a hydrogen bond with the 3-OH of the –2 sugar (glucose) residue, and along with Asn197 H-bonding to O4, is a key determinant of binding of GlcMan structures. The second invariant residue, Gly198, enables the formation of a 195 to 198 turn, thereby allowing residues 195, 196, and 197 to form hydrogen bonds with the –2 sugar (Fig. 3 *D* and *F*).

MANEA isolated from human liver carcinoma cells processes triglucosylated N-glycans at a lower rate than monoglucosylated N-glycans (9). In the GlcIFG complex of MANEA, the –2 loop is closed over the active site, and in this conformation, triglucosylated N-glycans are unable to bind to human MANEA. However, the other observed conformations show flexibility in the loop that could allow these extended structures to bind. Of note, bovine MANEA does not process triglucosylated N-glycans (9). While both bovine and human MANEA have the –2 loop, a Ser227 (human)-to-Lys change in the bovine enzyme was proposed to have contributed to the difference in specificity. Ser227 lies adjacent to and points toward the –2 loop, while the side chain of Lys226 (numbering as in bovine) may interact with the loop and reduce its mobility (Fig. 3*F*). Interactions with the loop may explain why CyMe-GlcIFG binds nearly 50-fold more weakly than GlcIFG. Notably, bacterial GH99 endomannanases, which act on complex extended yeast mannan substrates have open active sites and do not contain this loop (*SI Appendix*, Fig. S3). To test this hypothesis, we determined the structure of *Bx*GH99 with CyMe-GlcIFG (K_d of 339 nM; tighter binding than that of GlcIFG alone, 625 nM). The cyclohexyl ring is visible (but mobile) in the density, and indeed the loop in MANEA will occlude binding of the cyclohexyl group (*SI Appendix*, Fig. S4)

Human MANEA as a Host Cell Antiviral Target. To explore the potential of the endomannosidase pathway as an antiviral target, we studied the effect of MANEA inhibitors on replication of BVDV, a pestivirus of the *Flaviviridae* family. Reinfection assays showed that increasing concentrations of GlcIFG, the tightest-binding ligand of MANEA, resulted in a decrease in the number of infected cells (measured as focus-forming units [FFUs])

Fig. 4*A*. Previously, changes in the N-glycan structure of vesicular stomatitis virus (VSV) G protein induced by the MANEA inhibitor GlcDMJ were identified by demonstrating a change in susceptibility to hydrolysis by endo-β-*N*-acetylglucosaminidase (endo H) (41). Therefore, we digested BVDV envelope glycoproteins E1/E2 with endo H.

Increased sensitivity of E1/E2 proteins to endo H cleavage was observed in both GlcIFG and the glucosidase I/II inhibitor *N*-(6'-[4″-azido-2″-nitrophenylamino]hexyl)-1–deoxynojirimycin (NAP-DNJ), indicating an increased prevalence of high-mannose N-glycans. The increased sensitivity for GlcIFG was greater than that for NAP-DNJ, most likely reflecting the higher concentration of the former. Treatment with a combination of GlcIFG and NAP-DNJ provided an even greater sensitivity to endo H treatment, consistent with more effective cessation of N-glycan processing by blocking the glucosidase and endomannosidase pathways.

We next examined BVDV replication in the presence of a combination of GlcIFG and NAP-DNJ (Fig. 4*C*). These data showed that the combination of GlcIFG and NAP-DNJ gave a greater reduction than either agent alone, suggesting an additive antiviral effect from inhibiting both the α-glucosidase I/II and endomannosidase pathways. The addition of NAP-DNJ not only inhibits calnexin-mediated folding and quality control, but also requires viral glycans to undergo processing by MANEA, hence potentiating the antiviral effect.

To further define the antiviral potential of MANEA inhibitors, we extended these studies to DENV. The MANEA inhibitors GlcIFG, GlcDMJ, CyMe-GlcIFG, and ManIFG were used to study levels of viral particle formation and infectivity. Viral particle formation, as assessed by secreted viral RNA, was unaffected by treatment with MANEA inhibitors (Fig. 4*D*). However, treatment with GlcIFG, CyMe-GlcIFG, and GlcDMJ caused a reduction in plaque number, demonstrating that differences in glycosylation resulting from MANEA inhibition impair DENV infectivity. The greatest effect was seen for GlcDMJ, which reduced the number of plaque forming units by sixfold; ManIFG had no effect. The antiviral effect observed was at a relatively high concentration, but iminosugars are known to have difficulty in gaining access to the secretory pathway (21).

This proof-of-principle study demonstrates that GlcDMJ is a potential broad-spectrum antiviral, with changes in glycosylation reducing infectivity of the progeny. As it is the weakest-binding inhibitor, factors other than affinity, such as cell permeability, may be responsible for the potency of antiviral effects.

Summary

We report the 3D structure of Golgi MANEA, a eukaryotic N-glycosylation pathway glycosidase. The data provide a structural rationale for understanding the change in specificity of this enzyme for monoglucosylated, diglucosylated, and triglucosylated high-mannose N-glycans. We also show the potential for MANEA inhibitors to alter N-glycan structures of viral envelope glycoproteins and reduce viral infectivity. MANEA processes the $Glc_{1-3}Man_9GlcNAc_2$ structure and provides a pathway for glycoprotein maturation independent of the classical α-glucosidase I/II–dependent pathways. Treatment of HBV with miglustat (*N*-butyldeoxynojirimycin, an inhibitor of α-glucosidase II) impaired viral DNA secretion and led to aberrant N-glycans on M

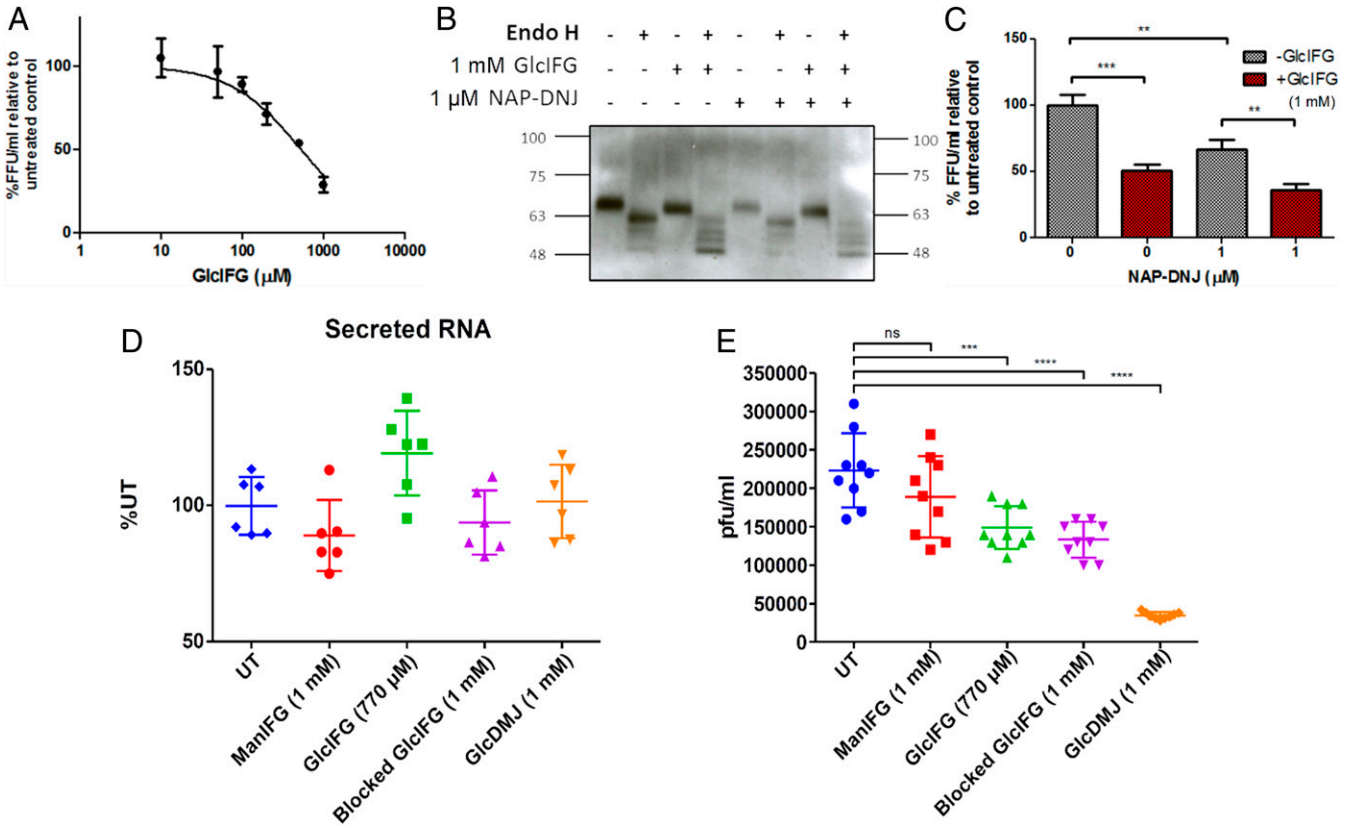

Fig. 4. Antiviral action of MANEA inhibitors. Results of BVDV reinfection assays in MDBK cells (*A*, *B*, and *C*) and DENV reinfection assays in Huh7.5 cells (*D* and *E*). (*A*) Percentage of FFU/mL relative to untreated cells at different concentrations of GlcIFG, at an MOI of 1. (*B*) Effect of MANEA inhibition (GlcIFG) and ER glucosidase II inhibition (NAP-DNJ) on the susceptibility of glycans on the BVDV E1/E2 protein to cleavage by endoH. (*C*) The combined effects of NAP-DNJ and GlcIFG on BVDV infectivity, as measured by FFU/mL. Experiments were performed in triplicate. (*D*) Secreted RNA levels in DENV-infected Huh7.5 cells. (*E*) Reinfectivity plaque assay from DENV-infected Huh7.5 cells. The horizontal bar in *D* and *E* indicates the mean.

glycoprotein, but other viral glycoproteins displayed mature glycans that arose through the endomannosidase pathway (23). Conversely, GlcDMJ treatment of VSV led to changes in G protein glycosylation (41).

These previous studies and the present work demonstrate that different viral glycoproteins have varying degrees of dependence on the α-glucosidase I/II and endomannosidase pathways for maturation, and that inhibition of MANEA alone can alter the infectivity of two encapsulated viruses. The human MANEA 3D structure along with the demonstrated antiviral activity of disaccharide imino and aza sugar inhibitors provide a foundation for future inhibitor and drug development work. Given the devastating consequences of global outbreaks of viral disease, the present work highlights the potential for MANEA as a new target for host-directed antiviral agents exploiting viral glycoprotein biosynthesis.

Methods

The methodology of this study is described in more detail in *SI Appendix*.

Expression, Characterization, and Structure Solution. In brief, recombinant MANEA-Δ97 featuring an N-terminal His tag was expressed in *E. coli* from a pColdI system coexpressing the *groEL* and *groES* genes encoding the GroEL/ES chaperone system. Recombinant MANEA-Δ97 was purified by metal-ion affinity and cation-exchange chromatography. Extensive crystal screening identified five different crystal forms, with a condition including 1 mM TEW allowing ligand-binding studies without an occluded active site. Structure solution by molecular replacement and refinement featured programs from the CCP4 suite (42). Structures and observed data have been deposited to the Protein Data Bank. MANEA activity was determined by mass spectrometry using $GlcMan_9GlcNAc_2$ as the substrate, with subsequent permethylation and analysis by matrix-assisted laser desorption/ionization mass spectroscopy. Michaelis–Menten kinetics was performed using a coupled assay with $GlcMan_3OMe$ as the substrate (30). Ligand-binding thermodynamics were determined by isothermal titration calorimetry.

Viral Infectivity Studies. Madin–Darby Canine Kidney (MDBK) cells were infected with BVDV at a multiplicity of infection (MOI) of 1, followed by incubation with different concentrations of GlcIFG (0 to 1 mM) and in combination with NAP-DNJ for 24 h. Cell culture medium was harvested, and serial dilutions were made and used to infect naive MDBK cells. Cells were incubated for 24 h, then washed and fixed with 4% (vol/vol) paraformaldehyde in PBS for 30 min. Following washing and blocking, cells were permeabilized and incubated with MAb103/105 (1:500 dilution in 5% milk-PBS; Animal Health Veterinary Laboratories Agency) for 1 h. Incubation with anti-mouse fluorescein isothiocyanate-conjugated secondary antibody (1:500 dilution in 5% milk-PBS; Sigma-Aldrich) and staining with DAPI allowed for the counting of fluorescent foci and calculation of virus titers (in FFU/mL). The samples obtained after treatment for 24 h were treated with Endo H and separated by sodium dodecyl sulfate polyacrylamide gel electrophoresis (SDS-PAGE) under nonreducing conditions. The membrane produced following transfer was probed with MAb214 primary antibody and then visualized with anti-mouse horseradish peroxidase secondary antibody (1:1,000; Dako) for 1 h.

Huh7.5 cells were infected for 2 h with 50 μL of DENV2 strain 16681 at an MOI of 0.1. The inoculum was removed and replaced with 200 μL of growth medium with drug at the indicated concentrations in triplicate, and the infected cells were incubated with drug for 2 d, after which the supernatant was harvested. DENV RNA in cell culture supernatants was isolated using the Direct-zol RNA MiniPrep Kit (Zymo Research) according to the manufacturer's protocol and then assayed by qRT-PCR. Samples were read in technical duplicate and compared with a standard curve generated from high-titer viral RNA isolated from C6/36-grown DENV2. The 95% confidence intervals were determined based on biological and technical variations and graphed using GraphPad Prism 6. The infectious DENV titers in supernatants collected were evaluated by a plaque assay.

Data Availability. All study data are included in the main text and *SI Appendix*.

ACKNOWLEDGMENTS. We thank Jon Agirre for assistance with generating a dictionary file for TEW, Eleanor Dodson for assistance with processing the highly anisotropic datasets, Alexandra Males for collecting ITC data with Glc-DMJ, and Mahima Sharma for assisting with supplemental figure production. We also thank Diamond Light Source UK for access to beamlines I03, I04, and I24 (Proposals mx1221, mx12587, and mx18598). Support for this work was provided by the European Research Council (ERC-2012-AdG-32294, "Glycopoise"), the Australian Research Council (DP120101396, FT130100103, and DP180101957), and the Royal Society (a Ken Murray Research Professorship, to G.J.D.).

1. M. Molinari, N-glycan structure dictates extension of protein folding or onset of disposal. *Nat. Chem. Biol.* **3**, 313–320 (2007).
2. A. Varki, Biological roles of glycans. *Glycobiology* **27**, 3–49 (2017).
3. K. Ohtsubo, J. D. Marth, Glycosylation in cellular mechanisms of health and disease. *Cell* **126**, 855–867 (2006).
4. J. Lombard, The multiple evolutionary origins of the eukaryotic N-glycosylation pathway. *Biol. Direct* **11**, 36 (2016).
5. M. Aebi, N-linked protein glycosylation in the ER. *Biochim. Biophys. Acta* **1833**, 2430–2437 (2013).
6. W. A. Lubas, R. G. Spiro, Evaluation of the role of rat liver Golgi endo-alpha-D-mannosidase in processing N-linked oligosaccharides. *J. Biol. Chem.* **263**, 3990–3998 (1988).
7. W. A. Lubas, R. G. Spiro, Golgi endo-α-D-mannosidase from rat liver, a novel N-linked carbohydrate unit processing enzyme. *J. Biol. Chem.* **262**, 3775–3781 (1987).
8. C. Zuber, M. J. Spiro, B. Guhl, R. G. Spiro, J. Roth, Golgi apparatus immunolocalization of endomannosidase suggests post-endoplasmic reticulum glucose trimming: Implications for quality control. *Mol. Biol. Cell* **11**, 4227–4240 (2000).
9. N. V. Kukushkin, I. S. Easthope, D. S. Alonzi, T. D. Butters, Restricted processing of glycans by endomannosidase in mammalian cells. *Glycobiology* **22**, 1282–1288 (2012).
10. S. E. Moore, R. G. Spiro, Demonstration that Golgi endo-alpha-D-mannosidase provides a glucosidase-independent pathway for the formation of complex N-linked oligosaccharides of glycoproteins. *J. Biol. Chem.* **265**, 13104–13112 (1990).
11. G. J. Gerwig *et al.*, A novel disorder caused by defective biosynthesis of N-linked oligosaccharides due to glucosidase I deficiency. *Am. J. Hum. Genet.* **66**, 1744–1756 (2000).
12. I. Bagdonaite, H. H. Wandall, Global aspects of viral glycosylation. *Glycobiology* **28**, 443–467 (2018).
13. M. A. Fischl *et al.*, The safety and efficacy of combination N-butyl-deoxynojirimycin (SC-48334) and zidovudine in patients with HIV-1 infection and 200-500 CD4 cells/mm^3. *J. Acquir. Immune Defic. Syndr. (1988)* **7**, 139–147 (1994).
14. A. C. Sayce *et al.*, Iminosugars inhibit dengue virus production via inhibition of ER alpha-glucosidases—not glycolipid processing enzymes. *PLoS Negl. Trop. Dis.* **10**, e0004524 (2016).
15. K. L. Warfield *et al.*, Targeting endoplasmic reticulum α-glucosidase I with a single-dose iminosugar treatment protects against lethal influenza and dengue virus infections. *J. Med. Chem.* **63**, 4205–4214 (2020).
16. X. Lu *et al.*, Aberrant trafficking of hepatitis B virus glycoproteins in cells in which N-glycan processing is inhibited. *Proc. Natl. Acad. Sci. U.S.A.* **94**, 2380–2385 (1997).
17. X. Lu, A. Mehta, R. Dwek, T. Butters, T. Block, Evidence that N-linked glycosylation is necessary for hepatitis B virus secretion. *Virology* **213**, 660–665 (1995).
18. R. A. Dwek, T. D. Butters, F. M. Platt, N. Zitzmann, Targeting glycosylation as a therapeutic approach. *Nat. Rev. Drug Discov.* **1**, 65–75 (2002).
19. J. Chang, T. M. Block, J. T. Guo, Antiviral therapies targeting host ER alpha-glucosidases: Current status and future directions. *Antiviral Res.* **99**, 251–260 (2013).
20. S. J. Williams, E. D. Goddard-Borger, α-glucosidase inhibitors as host-directed antiviral agents with potential for the treatment of COVID-19. *Biochem. Soc. Trans.* **48**, 1287–1295 (2020).
21. D. S. Alonzi, K. A. Scott, R. A. Dwek, N. Zitzmann, Iminosugar antivirals: The therapeutic sweet spot. *Biochem. Soc. Trans.* **45**, 571–582 (2017).
22. T. M. Block *et al.*, Secretion of human hepatitis B virus is inhibited by the imino sugar N-butyldeoxynojirimycin. *Proc. Natl. Acad. Sci. U.S.A.* **91**, 2235–2239 (1994).
23. A. Mehta, X. Lu, T. M. Block, B. S. Blumberg, R. A. Dwek, Hepatitis B virus (HBV) envelope glycoproteins vary drastically in their sensitivity to glycan processing: Evidence that alteration of a single N-linked glycosylation site can regulate HBV secretion. *Proc. Natl. Acad. Sci. U.S.A.* **94**, 1822–1827 (1997).
24. D. Dedera, N. Vander Heyden, L. Ratner, Attenuation of HIV-1 infectivity by an inhibitor of oligosaccharide processing. *AIDS Res. Hum. Retroviruses* **6**, 785–794 (1990).
25. D. A. Dedera, R. L. Gu, L. Ratner, Role of asparagine-linked glycosylation in human immunodeficiency virus type 1 transmembrane envelope function. *Virology* **187**, 377–382 (1992).
26. L. Ratner, N. van der Heyden, D. Dedera, Inhibition of HIV and SIV infectivity by blockade of α-glucosidase activity. *Virology* **181**, 180–192 (1991).
27. J. R. Francica *et al.*, Steric shielding of surface epitopes and impaired immune recognition induced by the Ebola virus glycoprotein. *PLoS Pathog.* **6**, e1001098 (2010).
28. V. Lombard, H. Golaconda Ramulu, E. Drula, P. M. Coutinho, B. Henrissat, The Carbohydrate-Active enZymes database (CAZy) in 2013. *Nucleic Acids Res.* **42**, D490–D495 (2014).
29. F. Cuskin *et al.*, Human gut Bacteroidetes can utilize yeast mannan through a selfish mechanism. *Nature* **517**, 165–169 (2015).
30. Z. Hakki *et al.*, Structural and kinetic dissection of the endo-α-1,2-mannanase activity of bacterial GH99 glycoside hydrolases from Bacteroides spp. *Chemistry* **21**, 1966–1977 (2015).

31. A. J. Thompson *et al*., Structural and mechanistic insight into N-glycan processing by endo-α-mannosidase. *Proc. Natl. Acad. Sci. U.S.A.* **109**, 781–786 (2012).
32. S. R. Hamilton *et al*., Intact alpha-1,2-endomannosidase is a typical type II membrane protein. *Glycobiology* **15**, 615–624 (2005).
33. S. Dedola *et al*., Direct assay for endo-α-mannosidase substrate preference on correctly folded and misfolded model glycoproteins. *Carbohydr. Res.* **434**, 94–98 (2016).
34. L. F. Sobala *et al*., An epoxide intermediate in glycosidase catalysis. *ACS Cent. Sci.* **6**, 760–770 (2020).
35. S. Hiraizumi, U. Spohr, R. G. Spiro, Characterization of endomannosidase inhibitors and evaluation of their effect on N-linked oligosaccharide processing during glycoprotein biosynthesis. *J. Biol. Chem.* **268**, 9927–9935 (1993).
36. U. Spohr, M. Bach, R. Spiro, Inhibitors of endo-alpha-mannosidase. 2. 1-deoxy-3-0-(alpha-D-glucopyranosyl)-mannojirimycin and congeners modified in the mannojirimycin unit. *Can. J. Chem.* **71**, 1928–1942 (1993).
37. D. S. Alonzi *et al*., Glycoprotein misfolding in the endoplasmic reticulum: Identification of released oligosaccharides reveals a second ER-associated degradation pathway for Golgi-retrieved proteins. *Cell. Mol. Life Sci.* **70**, 2799–2814 (2013).
38. H. Ardron *et al*., Synthesis of 1,5-dideoxy-3-O-(α-D-mannopyranosyl)-1,5-imino-D-mannitol and 1,5-dideoxy-3-O-(α-D-glucopyranosyl)-1,5-imino-D-mannitol: Powerful inhibitors of endomannosidase. *Tetrahedron Asymmetry* **4**, 2011–2024 (1993).
39. A. T. Caputo *et al*., Structures of mammalian ER α-glucosidase II capture the binding modes of broad-spectrum iminosugar antivirals. *Proc. Natl. Acad. Sci. U.S.A.* **113**, E4630–E4638 (2016).
40. A. Bijelic, A. Rompel, Ten good reasons for the use of the tellurium-centered Anderson-Evans polyoxotungstate in protein crystallography. *Acc. Chem. Res.* **50**, 1441–1448 (2017).
41. V. K. Karaivanova, P. Luan, R. G. Spiro, Processing of viral envelope glycoprotein by the endomannosidase pathway: Evaluation of host cell specificity. *Glycobiology* **8**, 725–730 (1998).
42. L. Potterton *et al*., CCP4i2: The new graphical user interface to the CCP4 program suite. *Acta Crystallogr. D Struct. Biol.* **74**, 68–84 (2018).
43. M. Shenkman, G. Z. Lederkremer, Compartmentalization and selective tagging for disposal of misfolded glycoproteins. *Trends Biochem. Sci.* **44**, 827–836 (2019).